ASEAN Journal of Chemical Engineering 2024, Vol. 24, No. 1, 36– 52

Catalytic Cracking of Oily Sludge using Nickel Metal Catalyst Embedded in Silica Derived from Adsorbent in a Gas Process Plant

Novita Jayanti [*,1]
Nazarudin [2]
Panut Mulyono [*,1]
[1] *Department of Chemical Engineering, Faculty of Engineering, Universitas Gadjah Mada, Yogyakarta 55281, Indonesia*
[2] *Department of Chemical Engineering, Faculty of Sains and Technology, University of Jambi, Jambi 36361, Indonesia*
[*]e-mail: novitajayanti096@gmail.com (N.J.); pmulyono@ugm.ac.id (P.M.)

Submitted 5 February 2024 *Revised* 6 March 2024 *Accepted* 15 March 2024

Abstract. One of the oily sludges (OS) recycling methods is through catalytic cracking. This process involves the reaction of breaking down large molecules into smaller ones with the help of a catalyst. Nickel (Ni) metal is often used as a catalyst because it can increase fuel liquid yield while reducing the coke formation. To enhance its performance, Ni metal can be embedded in a carrier material like Silica to form the Ni-Silica catalyst. In this research, OS sourced from a gas process plant is treated with catalytic cracking using Ni-Silica, where the silica used is derived from an adsorbent activated with NaOH. The cracking conditions are optimized using Response Surface Methodology (RSM) with a Box-Behnken design. The optimized cracking reaction conditions include temperature (713 K, 723 K, and 733 K), time (50 min, 60 min, and 70 min), and catalyst to OS ratio of 1:5, 1:6, and 1:7. Statistical analysis indicates that the relationship between the reaction condition variables and the oil liquid product (OLP) falls into the moderate category, as shown by the coefficient of determination (R^2) of 0.5. The calculated F-value for the deviation from the mathematical model is smaller than the F-Table value (9.2) at both 5% and 1% significance levels, with a value of 0.6. This indicates that the mathematical model generated can be accepted as the mathematical model within the range of reaction conditions in this study. Calculus analysis reveals that the optimum reaction conditions are a temperature of 717.34 K, a time of 58.58 min, and a catalyst to OS ratio of 1:6. Canonical analysis indicates that for OLP, λ_1= [-12.38], λ_2= [-2.27], and λ_3= [4.50], where lambda values indicate that the most sensitive response surface parameter for OLP is temperature, followed by the catalyst to sample ratio, and the least sensitive is reaction time.

Keywords: Catalytic Cracking, Ni Metal, Oily Sludge, RSM, Silica

INTRODUCTION

The oil and gas industry is known to produce one of its waste products, known as oily sludge (OS) (Murungi and Sulaimon 2022). The hydrocarbons contained in OS include aromatic hydrocarbons (25-40%), saturated hydrocarbons (40-60%), resins (10-15%), and asphalt (10-15%) (Hochberg *et al*., 2022). Based on its composition, OS is

DOI: 10.22146/ajche.10272

considered a potentially valuable energy source for recycling. One of the recycling methods used to produce fuel from OS is cracking (Lin *et al*., 2017a). Cracking is a thermal decomposition process that occurs without the use of oxygen. OS cracking can yield liquid, gas, and coke. Coke is the residue of cracking, while gas and Oil Liquid Product (OLP) are the products of cracking that have the potential to be used as fuel (Jin *et al*., 2021).

Cracking is a reaction of breaking down larger molecules into smaller molecules under specific operating conditions (Jia *et al*., 2017). One crucial operating condition to consider in the cracking process is temperature. For the cracking of OS, the appropriate temperature typically ranges from 600 K to 723 K, but it often requires a relatively long duration (Jin *et al*., 2021). Catalysts can be used to expedite the cracking process. Catalysts containing Nickel (Ni) are often used because they are cost-effective and readily available (Naidu *et al*., 2022, Tsiotsias *et al*., 2022). Nickel metal can be embedded in Silica, and this addition can modify the acidic sites when embedded in Silica, thereby enhancing the cracking yield (Ibrahim *et al*., 2021; Choi *et al*., 2022; Lin *et al*., 2017a; Lu *et al*., 2021). Catalysts based on Silica are often used in catalytic cracking processes because of their high conversion and selectivity towards the products (Wang *et al.,* 2017). Silica is also used as a catalyst because it possesses high acidity sites *(*Alnajjar *et al*., 2019).

In gas processing plants, the appeal of spent adsorbent is due to their silica content. XRD analysis reveals a crystalline structure supporting their catalytic function. Utilizing spent adsorbents in the catalytic cracking of OS yields high-quality oil liquid products. The catalyst derived from spent adsorbents in the gas processing plant has successfully enhanced catalytic cracking outcomes. The crystalline structure of these spent adsorbents presents new opportunities for developing industrial waste-based catalysts. This research is innovative for employing spent adsorbents as catalysts, diverging from conventional methods relying solely on waste as raw materials. Overall, feedstock and catalysts originate from the specific waste of the gas processing plant, marking a progressive step in efficiently and sustainably utilizing waste resources in the industry.

The feedstock for cracking is OS which researchers often use, the catalysts used are synthetic catalysts available for commercial purchase such as zeolite, dolomite, KOH and sillica (Zhang *et al*., 2022; Wang *et al*., 2017; Huang *et al*., 2015; Lin *et al*., 2017b). It is interesting to note no research has been conducted on OS and catalysts sourced from adsorbers in gas process plants, especially in Indonesia. One of the methods used for optimization in the research was Response Surface Methodology (RSM), using a Box-Behnken design. RSM determines the optimum operating conditions, including temperature, catalyst, and time. This research can potentially contribute valuable insights into the recycling of OS in the Indonesian context (Liu *et al*., 2021; Kasmin *et al.,* 2020; Zhang *et al*., 2022).

Oyebanji *et al.* (2023) have conducted research about the Box-Behnken design. It was employed with variations in temperature, biomass percentage, and catalyst percentage, without involving a specific duration for catalytic cracking. As a result, the exact cracking time remained unknown. In this research, we utilize the Box-Behnken design with temperature, time, and catalyst-to-sample ratio variations. This approach aims to determine the precise duration required for

catalytic cracking.

Therefore, in this study, optimization is conducted using RSM with a Box-Behnken design, utilizing feedstock and catalyst directly sourced from gas process plants in Indonesia. The variables that can be compared to the literature include lower cracking temperatures of 713 K, 723 K, and 733 K, operational times of 50 min, 60 min, and 70 min, as well as a catalyst to OS ratios of 1:5, 1:6, and 1:7. This research aims to provide insights into the optimal conditions for OS cracking in the specific context of the gas process plant. Herewith, the objective of the current study for the characteristics of spent catalyst adsorbents and new adsorbents from a gas process plant, which would subsequently be embedded with Nickel (Ni) metal for the catalytic cracking of oily sludge, was investigate.

MATERIALS AND METHODS

Materials

The materials used in this research were as follows: adsorbent and oily sludge, nitrogen gas 99% (PT. Rezeki Surya Gasindo), oxygen gas 99% (PT. Rezeki Surya Gasindo), hexane 99% (Sari Kimia), solid materials $Ni(NO_3)_2.9H_2O$ (Sigma Aldrich), solid NaOH 99% (Merck), and *aquadest*.

OS Preparation

Before conducting the OS cracking, a filtration treatment was performed using a Buchner funnel assisted by a vacuum pump to separate OS from water. The separated OS was mixed with hexane in a 1:1 ratio and stirred using a stirrer for 3 h at ambient temperature. During this stirring, oils present in the solid components of OS were expected to be released. Afterward, a second filtration was carried out using the same method described above, resulting in solid materials combined with OS.

After the second filtration, the separated OS was subjected to separation using a separating funnel for 15 min, resulting in two layers. The upper layer consisted of OS, while the lower layer was water. Following this, the OS in the upper layer underwent vacuum distillation for 2 h at a temperature of 342 K to separate hexane from OS. Afterward, the OS was obtained and was ready to be used as the feedstock for cracking.

Catalyst Preparation

Spent Adsorbent

The spent adsorbent was obtained from the used media of one of the adsorber units at Gas Process Plant. Prior to its use as a catalyst, a comparative analysis of the spent adsorbent was conducted against new adsorbents of types of MG-3 and MG-5. The spent adsorbent underwent a treatment process first. It was placed in a calcination reactor where oxygen gas was passed through it. Calcination was carried out at a temperature of 823 K for 5 h.

After calcination, the material was ground to obtain a powdered catalyst form. Subsequently, activation was performed using 1 M NaOH (NaOH Activation) with a spent adsorbent to NaOH ratio of 1:1. Activation was accomplished by stirring using a stirrer for 12 h at room temperature. Following this, filtration was conducted using a Buchner funnel aided by a vacuum pump and filter paper and a washing process until reaching a pH of 7. Afterward, drying was carried out in an oven for 12 h at 378 K. NaOH activation is used to clean the catalyst of contaminants that may have formed during storage or previous use. This helps restore or improve the activity of catalysts that may be affected by contamination or unwanted

buildup, thereby opening the pores of the catalyst (Lee *et al.*, 2021)

Embedding Nickel Metal on Spent Adsorbent through Hydrothermal Process

In this study, a Ni-adsorbent catalyst was prepared using a hydrothermal process. The procedure involved the dissolution of Ni-nitrate ($Ni(NO_3)_2.9H2O$) at a concentration of 2% in water, followed by incorporating the pre-prepared catalyst in an autoclave in a 1:10 ratio. Subsequently, the mixture was placed in an oven for 48 h at a temperature of 423 K. After the specified duration, the mixture was filtered, and the solid residue obtained on filter paper was then transferred to an oven for drying at 378 K for 12 h.

Cracking

Catalytic cracking of OS was carried out to produce OLP (Li *et al.*, 2021). Cracking is of breaking C-C bonds in long-chain, high molecular-weight hydrocarbons, transforming them into shorter-chain hydrocarbons with lower molecular weights. Cracking could occur under two main conditions: thermal and catalytic (Fakhroleslam and Sadrameli, 2019).

Nitrogen gas was employed as the product carrier gas. The variables used for cracking included the catalyst to OS ratio at 1:5, 1:6, and 1:7. Furthermore, OS was cracked in the cracking reactor under various conditions of temperature (713 K, 723 K, and 733 K) and reaction time (50 min, 60 min, and 70 min). The sequence of cracking reactors used in this study is presented in Figure 1.

Analysis of RSM

RSM is used to analyze the optimal conditions in this study. The OLP conversion value is a fixed variable (Y), while reaction conditions are treated as independent variables (X1 = temperature, X2 = time, and X3 = OS to catalyst ratio). This research involved optimization using RSM through the Matlab R2016b application.

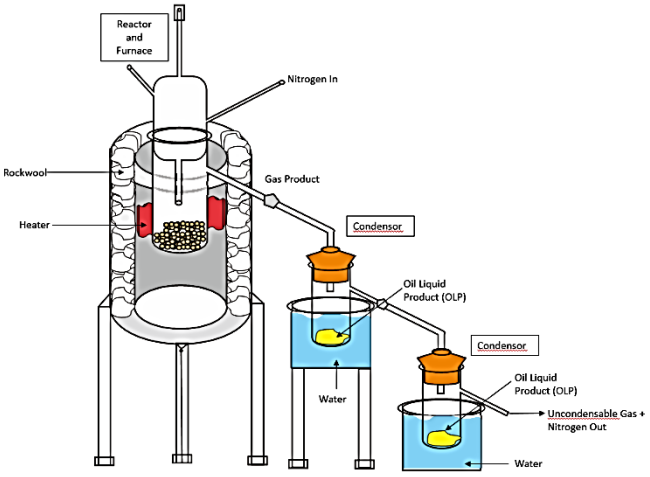

Fig. 1: Cracking equipment set-up utilized

RESULTS AND DISCUSSION

Analysis X-Ray Diffraction (XRD)

XRD analysis was conducted on the catalyst samples of the new adsorbent, MG-3 and MG-5, and on the spent adsorbent samples before and after calcination. This was carried out to determine the catalysts to be used in the subsequent OS catalytic cracking. The XRD results for the catalyst samples can be observed in Figures 2 and 3.

In Figure 2, labels (a) and (b), the red and black colors indicate that the XRD diffraction patterns formed are the amorphous type. From the XRD results of the label (a), it is evident that the peaks are distributed between 2θ values ranging from 20.36° to 26.89°. Likewise, from the XRD results of the label (b), it can be observed that the peaks are distributed between 2θ values ranging from 17.74° to 25.47°. The amorphous Silica peak broadens at around 20° in 2θ (Okoronkwo *et al.* 2016). For the spent adsorbent Catalyst, please refer to Figure 3.

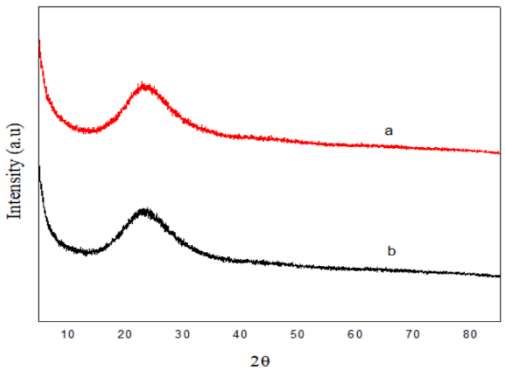

Fig. 2: Diffraction patterns of XRD; a) New Adsorbent MG-3; b) New Adsorbent MG-5.

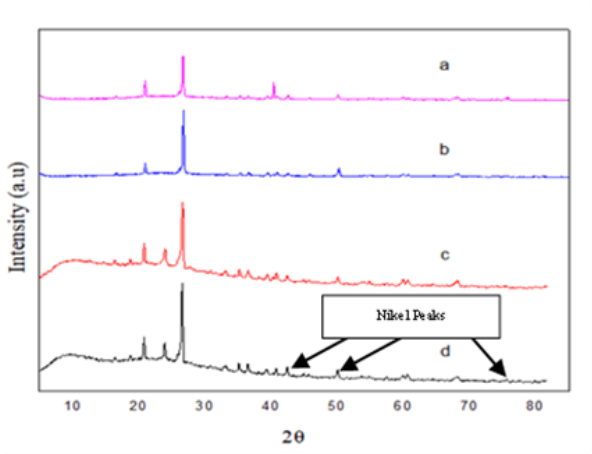

Fig. 3: Diffraction patterns of XRD;
a) *Spent adsorbent before calcination*;
b) *Spent adsorbent after calcination*;
c) *Spent adsorbent after calcination, followed by activation with NaOH*;
d) *Spent adsorbent after calcination, treated with NaOH activation, and subjected to hydrothermal treatment* (Ni 2%)

In Figure 3, label (a) in purple shows the highest peaks at 2θ values of 21.01°, 26.70°, and 40.41°. Label (b) in blue exhibits the highest peaks at 2θ values of 20.99°, 26.71°, and 50.26°. According to Okoronkwo *et al.* (2016), the presence of peaks at 2θ around 20° indicates the presence of Silica. This aligns with the highest peaks at 2θ formed from the XRD results of the label (a), specifically at 21.01° and 26.70° for the non-calcined spent adsorbent. The change in diffraction pattern for this spent adsorbent is attributed to the heating process it underwent in the gas process plant, where it was heated to a temperature of 293°C.

This heating transformed the diffraction pattern of the adsorbent from amorphous to crystalline. As for the calcined spent adsorbent, the 2θ values obtained were 20.99° and 26.71°. The difference in intensity at 20.99° and 21.01°, as well as 26.70° and 26.71° can be attributed to the presence of deposits that either detach from or cover the pore surface. In labels (c) in red and (d) in black, a change at the beginning of the pattern compared to labels (a) and (b) can be observed. This change is due to the catalyst activation process, which opens the catalyst pores and causes deposits adhering to the catalyst surface to detach (Nazaruddin *et al.*, 2020).

Catalysts require the right level of acidity to produce the desired products. Therefore, on the catalyst that has already been activated with NaOH, a hydrothermal process with nickel was carried out to increase the acidity. Consequently, in label (d) in black, peaks of Nickel metal can be observed at 2θ values of 44.5°, 51.8°, and 76.4°, indicating the presence of nickel metal (Amin, 2020).

From the explanation above, Figure 2 and Figure 3 differ. Figure 2 represents the XRD results for the new adsorbent, revealing its amorphous structure following XRD analysis. On the other hand, Figure 3 illustrates the XRD results for the spent adsorbent, indicating its crystalline structure after XRD analysis. Both can be utilized as catalysts, whether amorphous or crystalline, depending on the specific catalytic requirements. This journal employs the spent adsorbent with a crystalline structure as a catalyst.

The treatment of the catalyst using NaOH can destroy crystallinity because

NaOH is a base that can disrupt the crystal structure. When the catalyst comes into contact with a NaOH solution, OH- ions from the alkaline solution can react with the catalyst's surface, disrupting the bonds between particles in the crystal structure of the catalyst. This process changes to the catalyst's structure (Triyono, 2023). FTIR analysis was conducted to assess the acidity level of the catalyst.

Analysis Fourier Transform Infra-Red (FTIR)

FTIR analysis was conducted on the samples of spent adsorbent after calcination, treated with NaOH activation, and subjected to hydrothermal treatment with 2% Ni for 1 day, 2 days, and 3 days. This was performed to select the most suitable catalyst for OS cracking. The FTIR spectra results can be observed in Figure 4.

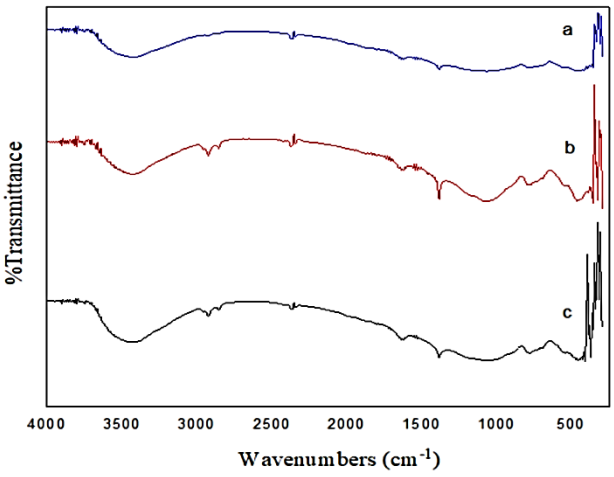

Fig 4. FTIR Spectra of spent adsorbent after calcination, treated with NaOH activation, and subjected to hydrothermal treatment (Ni 2%); a) 1 day; b) 2 days; c) 3 days.

In Figure 4, labels (a) in blue, (b) in red, and (c) in black indicate the presence of absorption peaks between 3200 – 3500 cm^{-1}, indicating the presence of OH groups (Sharma *et al.*, 2018). Subsequently, the absorption of 400 – 500 cm^{-1} indicates the presence of Nickel in the catalyst (Amin, 2020). From Figure 4, label (b) in red with a 2-day Hydrothermal treatment was subjected to further analysis for use as a catalyst in this study. This choice was made due to its higher acidity, as evidenced by the increased OLP yield compared to the catalysts subjected to hydrothermal treatment for 1 day and 3 days in the OS cracking experiments.

FTIR analysis without the presence of Ni was not conducted such as Saravanan and Dubey, 2020 and Tran *et al.*, 2013 for FTIR results regarding Silica, as shown in Figure 5.

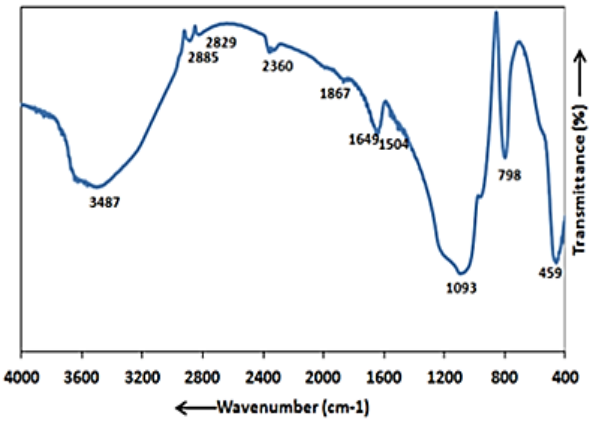

Fig. 5: FTIR analysis without Ni.

Figure 5 shows that the FTIR analysis showed an identical pattern in Figure 4, except for variations in peaks of 400–500 cm^{-1}. So, when nickel is embedded into the adsorbent, it can be ascertained that the peak of 400 - 500 is the peak of nickel.

Analysis Scanning Electron Microscope-Energy Dispersive X-Ray (SEM-EDX)

SEM-EDX analysis was performed on samples of spent adsorbent catalyst before calcination, spent adsorbent catalyst after calcination followed by NaOH activation, and spent adsorbent catalyst after calcination,

NaOH activation, and hydrothermal treatment (Ni 2%) for 2 days. The SEM-EDX results for the catalyst samples are presented in Figure 6 and Figure 7.

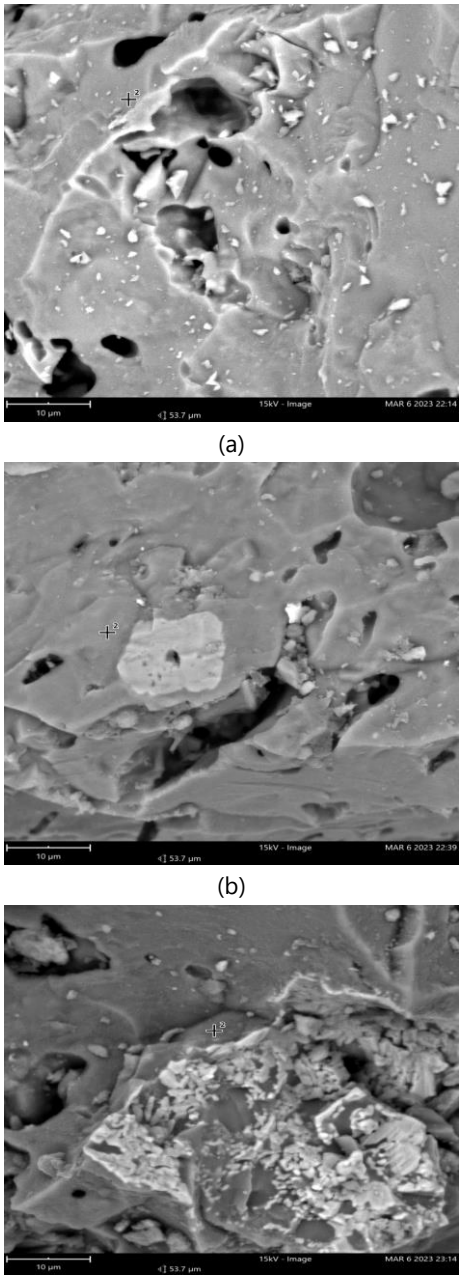

(a)

(b)

(c)

Fig. 6: Figure SEM for EDX *(SEM-EDX Image)*; a) Spent adsorbent before calcination; b) Spent adsorbent after calcination, followed by activation with NaOH; c) Spent adsorbent after calcination, activated with NaOH and subjected to hydrothermal treatment (Ni 2%) for 2 days

In Figure 6, labels (a), (b), and (c) depict SEM images of each adsorbent with different treatments. Label (a) shows that the pores in the catalyst are not yet open, and impurities covering the catalyst pores are still visible. In label (b), the pores in the catalyst appear open, and impurities are reduced. Label (c) shows scattered Ni metal within the catalyst pores. For its composition, please refer to Figure 7.

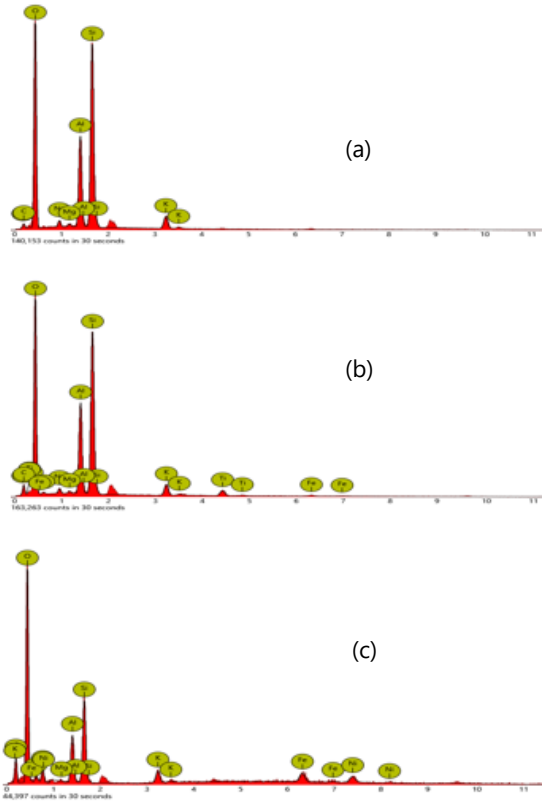

(a)

(b)

(c)

Fig. 7: EDX spectra; a) Spent adsorbent before calcination; b) Spent adsorbent after calcination, then activated with NaOH; c) Spent adsorbent after calcination, activated with NaOH, and subjected to hydrothermal treatment (Ni 2%) for 2 days

In Figure 7, labels (a), (b), and (c) display the EDX spectra corresponding to the SEM images of each adsorbent with different treatments. Tabel 1 provides the percentage composition (%) obtained from the EDX results.

Table 1. Elements SEM-EDX

Element Name	Labels a (%)	Labels b (%)	Labels c (%)
Oxygen	42.44	49.90	55.26
Silica	47.40	39.81	32.77
Aluminum	8.36	7.82	4.57
Potassium	1.21	1.10	1.26
Sodium	0.38	0.51	-
Magnesium	0.22	0.27	0.1
Iron	-	0.29	2.86
Titanium	-	0.28	-
Nickel	-	-	3.16

From Table 1, it can be observed that in the label (a), the silica content is 47.40%. In label (b), the silica content is 39.81%, and it can also be observed that were several metals detected. These metals are likely deposits trapped within the catalyst pores, and during activation, they are released from the catalyst pores. In label (c), the presence of nickel is noted at 3.16%, and the Silica content decreases to 32.77%. This is attributed to the loss of some structural cations, leading to a decline in catalyst stability and the breakdown of the catalyst structure (Nazaruddin *et al*., 2020).

Gas Chromatography-Mass Spectrometry (GC-MS) Analysis on Raw Materials.

The pre-prepared OS underwent analysis using Gas Chromatography-Mass Spectrometry (GC-MS) to identify the number of carbon atoms and the major component by percentage and predict the names of compounds in the OS. GC can quantitatively analyze the number of compounds, while MS can determine component's types. The results of the GC-MS analysis on the OS samples can be found in Table 2.

Table 2. Results of GC-MS analysis of OS after treatment

No	RT	%Area	SI	Compound Name	Molecular Formula	Molecular-Weight
1	2.045	17.17	94	Methyl cyclopentane	C_6H_{12}	84
2	24.547	3.04	95	Undecane	$C_{11}H_{24}$	156
3	26.096	1.84	94	Tetradecane	$C_{14}H_{30}$	198
4	27.198	4.17	96	Tetradecane	$C_{14}H_{30}$	198
5	29.706	4.34	96	Tetradecane	$C_{14}H_{30}$	198
6	30.769	1.85	95	Dodecane	$C_{12}H_{26}$	170
7	32.089	11.57	95	Pentadecane	$C_{15}H_{32}$	212
8	34.340	5.68	96	n-Tetradecane	$C_{14}H_{30}$	198
9	36.489	4.15	96	Tetradecane	$C_{14}H_{30}$	198
10	38.538	4.24	96	Tetradecane	$C_{14}H_{30}$	198
11	40.494	3.87	96	Tetradecane	$C_{14}H_{30}$	198
12	42.370	4.06	95	Tetradecane	$C_{14}H_{30}$	198
13	44.169	4.05	95	Tetradecane	$C_{14}H_{30}$	198
14	45.893	4.16	94	Pentadecane	$C_{15}H_{32}$	212
15	47.554	3.75	94	Tetradecane	$C_{14}H_{30}$	198
16	49.151	4.31	94	n-Nonadecane	$C_{19}H_{40}$	268
17	50.691	4.19	94	n-Nonadecane	$C_{19}H_{40}$	268
18	52.175	3.63	94	n-Nonadecane	$C_{19}H_{40}$	268
19	53.608	3.58	93	n-Nonadecane	$C_{19}H_{40}$	268
20	54.994	2.62	93	n-Nonadecane	$C_{19}H_{40}$	268
21	26.337	2.29	93	n-Nonadecane	$C_{19}H_{40}$	268
22	59.148	1.44	90	Nonadecane, 2-methyl	$C_{20}H_{42}$	282

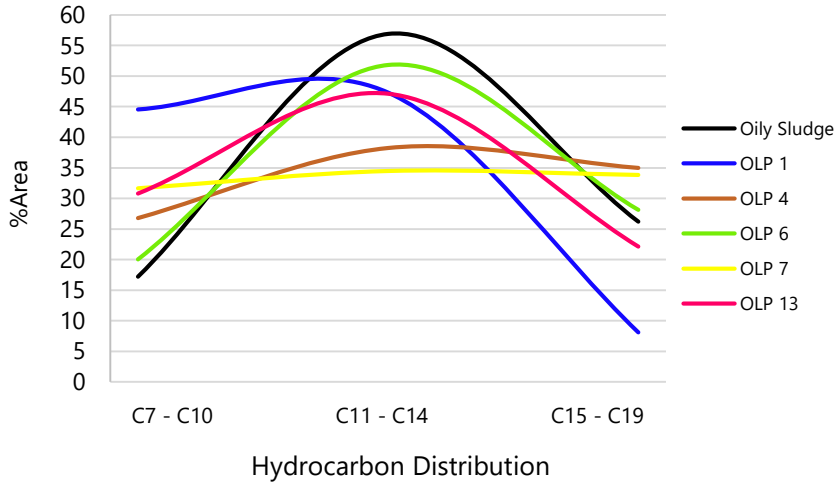

Fig. 8: Hydrocarbon distribution in OLP 1 – OLP 15

Table 2 shows that identifying compound components in the OS resulted in 22 peaks. Based on the GC-MS analysis, it can be concluded that the compounds contained have carbon atoms ranging from C6 to C20. This analysis also reveals that the highest % area corresponds to peaks 1 and 7, indicating a significant percentage of these compounds.

Catalytic cracking of OS produces OLP, which will then be analyzed using GC-MS to identify the number of carbon atoms and the major component by percentage and predict the names of compounds in OLP. The GC-MS results for OLP can be seen in Figure 8.

Cracking has been carried out in many previous studies, one of which, Jin et al., 2021, has carried out thermal cracking of OS where the results obtained are that OLP increases when the temperature starts from 723 K, reaching a peak at 76.84% by weight at 750 ◦C. The yield then decreases with increasing temperature due to the increase in the gas. Meanwhile, for time, OLP increased from 74.91% by weight to 76.84% as the reaction time increased from 15 minutes to 60 minutes at a cracking temperature of 1023 K. This shows that the cracking time was relatively long. The temperature used was relatively high for producing OLP. The OLP content obtained is high in heterocyclic oxygen and not too much hydrocarbon.

From the above explanation, a catalyst is necessary to reduce the cracking temperature and obtain OLP which contains a lot of hydrocarbons. So, in this research, the use of a catalyst is needed; the catalyst used in this research is Ni-Adsorbent and produces OLP with a hydrocarbon distribution as in Figure 8.

Research related to the cracking of OS is also conducted by Lin *et al.* (2017). Obtaining a hydrocarbon distribution of C_{14}-C_{24} below 35% in the cracking of OS, conducted by Lin *et al.* (2017) Using KOH catalyst with concentrations of 5% and 10% at a temperature of 600 °C and a duration of 60 min, the hydrocarbon chains of C_{14}-C_{24} were found to be 34.8% and 33.6%, respectively, in the OS cracking process.

Figure 8 shows that for the distribution of hydrocarbons C_{15}-C_{19} in OLP 1 - OLP 15, the values are not more than 35%. Additionally, in Figure 8, it can be seen that OLP 1, operating at 713 K, 60 min, and with a catalyst-to-OS ratio of 1:6, has a low content of hydrocarbons C_{15}-C_{19}, which is 8.13%. This indicates that almost all hydrocarbons are being cracked into shorter hydrocarbon chains. However, when using a KOH catalyst

at a higher temperature, there is still a significant presence of hydrocarbon chains C_{14}-C_{24}, with a value of 33.6%.

From the above explanation, it suggests that there are still a substantial amount of Hydrocarbon chains that have not undergone cracking into shorter hydrocarbons. This implies that the OLP 1 - OLP 15 content in Figure 8 can be considered to have experienced cracking into shorter hydrocarbons. This is further supported by the increased percentage of $C_7 – C_{10}$ in OLP 1 - OLP 15 compared to the feedstock.

Additionally, for hydrocarbons $C_{11} – C_{14}$, OLP 1 - OLP 15 have lower concentrations than the feedstock. This explanation demonstrates that catalytic cracking has been successful, as evidenced by the distribution of hydrocarbons trending towards lighter hydrocarbons compared to the feedstock (OS). Furthermore, the Ni-Adsorbent catalyst appears to be effective in catalyzing the cracking of OS, leaving behind only a small amount of C_{15}-C_{19} hydrocarbon chains.

Figure 8 shows the highest distribution of hydrocarbons for feedstock (OS) is $C_{11} – C_{14}$. Then, the OS is cracked from the long hydrocarbon to the short hydrocarbon. The cracking product in this research is called OLP, which is expected to have a hydrocarbon distribution in C_7 - C_{10}. In the research, 15 variations of cracking were carried out using a Ni-Adsorbent catalyst to produce 15 OLP. In Figure 8, several samples were selected that could represent the lower conditions, middle conditions, and expected conditions.

For lower conditions with a hydrocarbon distribution of $C_7 – C_{10}$ of 20.04%, $C_{11} – C_{14}$ of 51.83% and $C_{15} – C_{19}$ of 28.14% found in OLP 6 (operating conditions 713 K, 60 minutes and catalyst-to-OS 1:7). For middle conditions, namely OLP 7 (operating conditions 733 K, 60 minutes, and catalyst per sample 1:5) produces $C_7 – C_{10}$ of 31.65%, $C_{11} – C_{14}$ of 34.50% and $C_{15} – C_{19}$ of 33.85%. For the expected hydrocarbon distribution, OLP 1 (operating conditions 713 K, 60 minutes and catalyst per OS 1:6) and OLP 13 have the highest $C_7 – C_{10}$ values with values of 44.55% and 30.79% and produce $C_{11} – C_{14}$ and $C_{15} – C_{19}$ 8.13%.

Furthermore, when examining the cracking of OS resulting in OLP 1 - OLP 15 in Figure 8 under various operating conditions, the hydrocarbon distribution obtained can be classified as fuel. For C_5-C_{10}, it falls into the gasoline category with a boiling point range of 303 K - 453 K. From the research findings, the highest concentration in this range is observed in OLP 1 under the operating conditions of 713 K, 60 min, and a catalyst per OS ratio of 1:6.

The classification of fuel in the C_{11}-C_{12} range falls into the kerosene category with a boiling point range of 453 K - 503 K. From the research results, the closest match to this category is found in OLP 6 under the operating conditions of 713 K, 60 min, and a catalyst per OS ratio of 1:7. The classification of C_{13}-C_{17} falls into the diesel category with a boiling point range of 503 K - 578 K, and C_{18} falls into the heavy fraction category with a boiling point range of 578 K - 678 K. From the research findings, the highest concentration in the C_{13}-C_{17} range is observed in OLP 4 under the operating conditions of 733 K, 70 min, and a catalyst per OS ratio of 1:6.

From the above explanation, it can be concluded that operating conditions such as temperature, time, and the catalyst-to-OS ratio influence the type of fuel produced and can be known as cracking due to temperature and the influence of catalysts differentiate the hydrocarbons obtained. When using a catalyst, the reaction is more directed, and the resulting products tend to be

homogeneous hydrocarbons with lower carbon chain lengths. On the other hand, cracking due to temperature yields longer-chain or non-homogeneous hydrocarbons, and the reactions are typically less controlled.

Optimizing Catalytic Cracking Reactions Using Response Surface Methodology RSM

The results of catalytic cracking with the Box-Behnken design used in this study can be seen in Table 3. Table 3 shows that the OS cracking process produces OLP, gas, and coke, with the percentage of OLP as the response variable (Y) to be further analyzed using RSM.

Analysis of RSM on Data of OS Catalytic Cracking using Used Ni-Adsorbent

From this analysis, regression coefficients on OLP are obtained and can be incorporated into a second order mathematical model as described by Equation 1.

$$Yi = 60{,}67 + 9{,}6X_1 - 5{,}37X_2 - 6{,}74X_3 + 1{,}37X_1X_2 - 8{,}4X_1X_3 - 7{,}21X_2X_3 + 2{,}01{X_1}^2 + 12{,}99{X_2}^2 - 11{,}91{X_3}^2 \quad (1)$$

The regression coefficients of the second-order equation with the percentage yield of OLP can be observed in Figure 9.

Table 3. The Results of catalytic cracking using the Box-Behnken design

No	Reaction Conditions			Cracking Yield (%)
	Temperature (K)	Time (Min)	Catalyst to Feed Ratio	OLP
1	713	50	1:6	68.58
2	713	70	1:6	67.42
3	733	50	1:6	73.75
4	733	70	1:6	72.38
5	713	60	1:5	57.50
6	713	60	1:7	47.21
7	733	60	1:5	79.67
8	733	60	1:7	57.84
9	723	50	1:5	42.75
10	723	50	1:7	66.54
11	723	70	1:5	41.13
12	723	70	1:7	65.21
13	723	60	1:6	74.13
14	723	60	1:6	76.63
15	723	60	1:6	54.54

In Figure 9, the regression coefficients are absolute values, and it can be observed that the coefficient for X_1 is the highest among X_2 and X_3. From these regression coefficients, the graph for X_1*X_3 is also high, indicating that both X_1 and X_3 influence the OLP percentage.

The regression coefficients in Table 3 underwent analysis of variance (ANOVA) as in Table 4

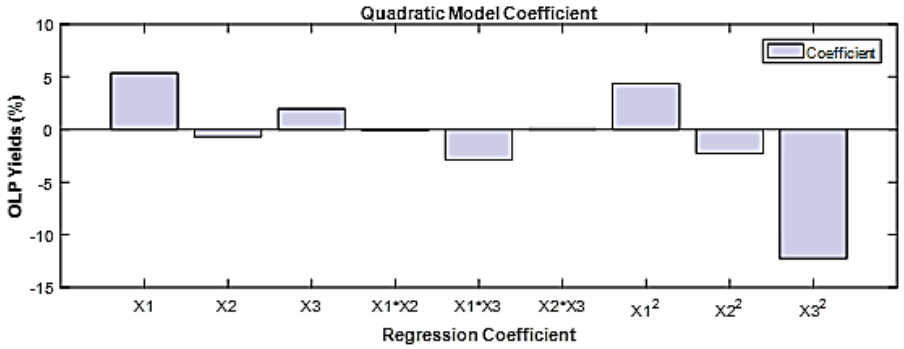

Fig. 9: Regression coefficient graph of second-order equation against OLP percentage

.

Table 4. ANOVA

Source of Variation	OLP
SS	968.58
df	9.00
MS	107.62
F	1.97
P-value	0.48
F Table	19.38
R^2	0.46

Table 4. reveals that the coefficient of determination (R^2) for OLP is 0.46. This R^2 value indicates the correlation between Y and X. The R^2 value for OLP suggests a medium correlation. The analysis of variance also demonstrates that the calculated F-value for the deviation from the mathematical model in Table 3 is smaller than the critical F Table value (9.2) at α=0.05 and α=0.01.

From this presentation, the R^2 value for OLP tends to be medium, and the calculated F-value is smaller than the F Table value (9.2). This indicates that Equation 4 with the regression coefficients in Table 3 is appropriate as the equation for this study. Furthermore, the optimum conditions for the OLP variable X_1 are found to be -1.93 with an optimum condition of 703.69 K, for variable X_2 the value is 0.39 with an optimum condition of 63.86 min, and for variable X_3, the value is 0.28 with an optimum condition of 6.28:1.

The predicted OLP percentage under these optimum operating conditions is 49.41%. Canonical analysis was also conducted in this study to determine the sensitivity of the independent variables to the dependent variable, where the value of λ is an absolute value. The graph of the canonical analysis can be seen in Figure 10.

In Figure 10, it can be observed that the results for OLP are obtained λ_1= [-13,49], λ_2= [2,93] and λ_3= [-13,65], This indicates that the response surface most sensitive to OLP in this study is the catalyst-to-sample ratio, followed by temperature, while reaction time appears to be the least sensitive.

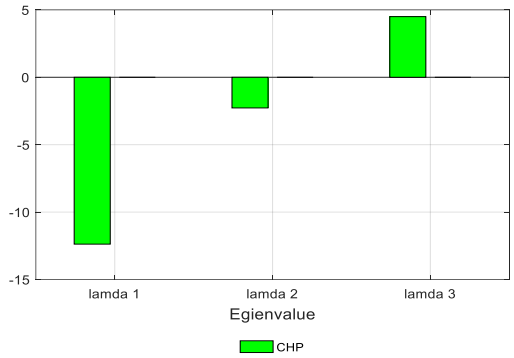

Fig. 10: Chart λ_1, λ_2 and λ_3

Surface Graph and Contour Graph in RSM Analysis

Figure 11 shows surface graphs and contour graphs depicting the relationship between temperature and reaction time with respect to the percentage of OLP yield. Similarly, Figure 12 displays the surface and contour graphs illustrating the correlation between temperature and catalyst-to-OS ratio about the percentage of OLP yield. Lastly, Figure 13 presents the surface and contour graphs showcasing the connection between reaction time and the catalyst-to-OS ratio concerning the percentage of OLP yield.

In Figure 11, symbol (a) displays a graph depicting the relationship between temperature and reaction time concerning OLP, derived from catalytic cracking data, forming a saddle-shaped graph. This implies that the optimum point between temperature and reaction time is not a single point but rather scattered across a saddle-shaped region. Symbol (b) represents a contour graph, which serves the purpose of aiding in the interpretation of the surface graph and confirming the type of surface graph. In symbol (b), you can observe that the lines formed do not create circles, indicating that this graph forms a saddle-shaped pattern.

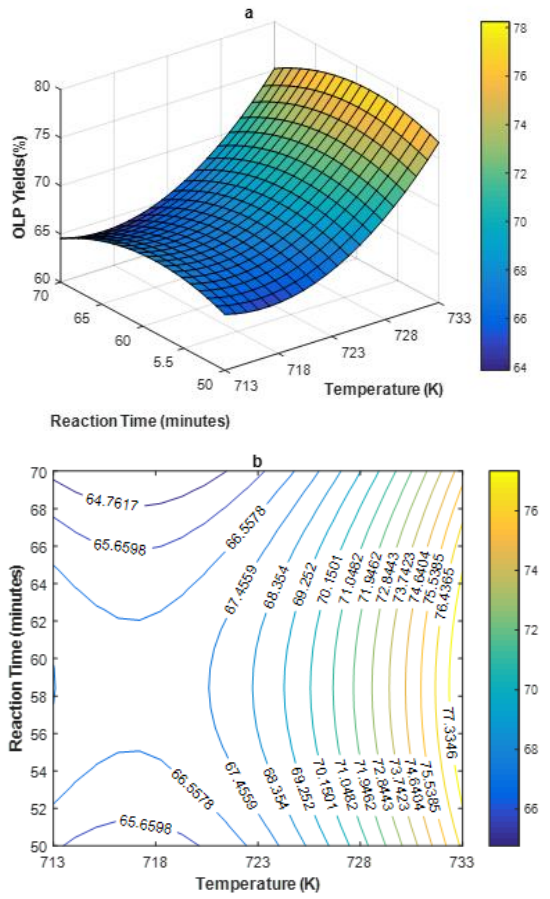

Fig. 11: a) Surface graph of temperature and reaction time against OLP; b) Contour graph of temperature and reaction time against OLP

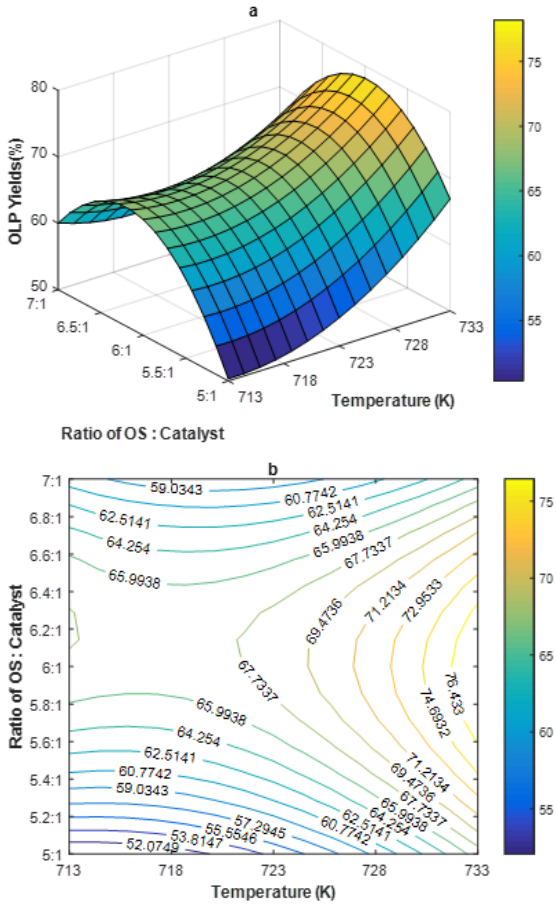

Fig. 12: a) Surface graph of temperature and catalyst-to-OS ratio against OLP; b) contour graph of temperature

In Figure 12, symbol (a) displays a graph illustrating the relationship between temperature and the catalyst-to-OS ratio concerning OLP, derived from catalytic cracking data, forming a saddle-shaped graph. This indicates that the optimal point between temperature and the catalyst-to-OS ratio is not a single point but is scattered across a saddle-shaped region. Symbol (b) represents a contour graph, facilitates the interpretation of the surface graph and confirms the type of surface graph. In symbol (b), you can observe that the lines formed do not create circles, indicating that this graph forms a saddle-shaped pattern.

In Figure 13, symbol (a) displays a graph depicting the relationship between reaction time and the catalyst-to-OS ratio concerning OLP, derived from catalytic cracking data, forming a type of maximum optimum graph. This means that the optimal point between reaction time and the catalyst-to-OS ratio is at the maximum peak value depicted in Figure 13. Symbol (b) represents a contour graph, which serves the purpose of aiding in the interpretation of the surface graph and confirming the type of surface graph. In symbol (b), you can observe that the lines formed resemble circles, indicating that this graph indeed forms a maximum optimum pattern.

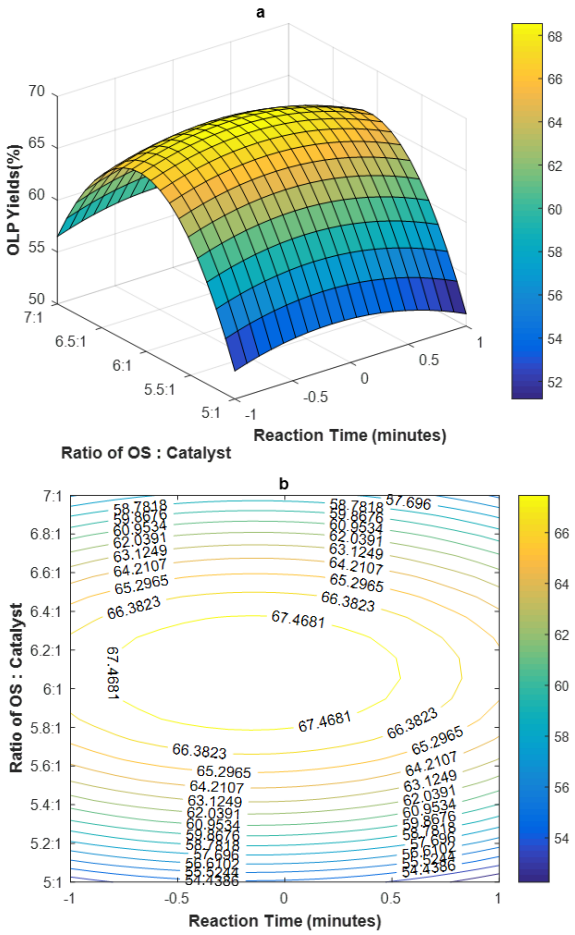

Fig. 13: a) Surface graph of time and catalyst-to-OS ratio against OLP; b) Contour graph of time and catalyst-to-OS ratio against OLP

Table 5 provides a comprehensive overview of the RSM analysis from the above explanation. It is evident from Table 5 that all mathematical models obtained using RSM are acceptable. Furthermore, the sensitivity analysis for OLP indicates that the most sensitive response surface for OLP is temperature, followed by catalyst-to-sample ratio, with reaction time being the least sensitive factor. The RSM analysis also identifies the optimum reaction conditions for the catalytic cracking study using used(?) Ni-Adsorbent, as shown in Table 6.

Table 6 provides the optimal operating conditions obtained from the RSM analysis. The prediction and experimental results of OS cracking using the optimal operating conditions from the RSM analysis only differ by 5.98%. According to Mahfeli (2022), the acceptable difference between prediction and experimental results for RSM analysis is below 10%. This indicates that RSM analysis can be used for OS cracking optimization since the obtained difference falls within the allowable range.

Table 5. RSM analysis results

Results (Y)	Statistical Parameters			Accepted or Rejected Model	Canonical Analysis			Sensitivity	Type of Graph		
	R^2	F Calculate	F Table (9.2)		λ_1	λ_2	λ_3		X_1X_2	X_1X_3	X_2X_3
		LF	α = 0.05	α = 0.01							
OLP	0.46	1.97	19.38	99.38	Accepted	-12.38	-2.27	4.50	t<ks<T	*Saddle*	*Saddle*	Maximum

Table 6. Optimal operating conditions

No	Conversion for	Optimal Variable Values			OLP	
		Temperature (Kelvin)	Time (Min)	K/S	Prediction	Verification
1	OLP	717.34	58.58	1:6.15	67.10%	73.08%

CONCLUSION

The Ni-adsorbent (spent) was repurposed as a catalyst in catalytic cracking. XRD analysis for the new adsorbent is amorphous, while the spent adsorbent is crystalline. Consequently, this research chose the Ni-Adsorbent (spent) as a catalyst. FTIR analysis indicated that the Ni-adsorbent (spent) catalyst subjected to 2 days of hydrothermal treatment was the most suitable. SEM EDX analysis observed that the Ni-Adsorbent treated with a 2-day hydrothermal process exhibited a well-dispersed distribution of Nickel.

The highest OLP yield achieved of OLP 7 (temperature of 733 K, time of 60 minutes, and a catalyst-to-OS ratio of 1:5) is 79.67%. The Analysis of GC-MS in OLP 1, the expected hydrocarbon distribution (operating conditions 713 K, 60 minutes, and catalyst per OS 1:6) of $C_7 - C_{10}$ values are 44.55% and 30.79%. With the design of *Box-Behnken*, RSM can provide the precise mathematical equation to determine the optimal operating conditions (temperature, time, and catalyst-to-OS ratio) to ascertain the optimum OLP yield. Upon confirmation of the predicted optimum OLP value and experimental results, a minimal difference of only 6% was observed. Hence, it can be concluded that the RSM analysis yields accurate predictions for this OS cracking process.

ACKNOWLEDGEMENT

We would like to express our heartfelt gratitude to our thesis advisor, academic mentor, the Department of Chemical Engineering at Universitas Gadjah Mada, the PS-ENAM Laboratory at Universitas Jambi, and one of Indonesia's Oil and Gas companies. Your guidance and support have been invaluable throughout our research journey.

NOMENCLATURE

X_1 or T or λ_1	:	Temperature (K)
X_2 or t or λ_2	:	Time (min)
X_3 or k/s or λ_3	:	Ratio of catalysts per OS (gr)
β	:	Regression Coefficients

REFERENCES

Alnajjar, M., Hethnawi, A., Nafie, G., Hassan, A., Vitale, G., and Nassar, N.N., 2019. "Silica-alumina composite as an effective adsorbent for the removal of metformin from water." *J. Environ. Chem. Eng. 7*, 1–10.

Amin, M.H., 2020. "Relationship between the pore structure of mesoporous Silica supports and the activity of Nickel nanocatalysts in the CO_2 reforming of methane." *Catalysts 10*, 1–21.

Choi, D.S., Kim, J., Kim, N.Y., and Joo, J.B., 2022. "Control of textural property in spherical alumina ball for enhanced catalytic activity of Ni-supported Al_2O_3 catalyst in steam–methane reforming." *J. Ind. Eng. Chem. 108*, 400–410.

Fakhroleslam, M., and Sadrameli, S.M., 2019. "Thermal/catalytic cracking of hydrocarbons for the production of olefins; a state-of-the-art review III: Process modeling and simulation." *Fuel 252*, 553–566.

Gea, S., Haryono, A., Andriayani, A., Sihombing, J.L., Pulungan, A.N., Nasution, T., Rahayu, R., and Hutapea, Y.A., 2020. "The effect of chemical activation using base solution with various concentrations towards sarulla natural zeolite." *Elkawnie 6*, 85.

Hochberg, S.Y., Tansel, B., and Laha, S., 2022. "Materials and energy recovery from OSs removed from crude oil storage tanks (tank bottoms): A review of technologies." *J. Environ. Manage. 305*, 114428.

Huang, Q., Wang, J., Qiu, K., Pan, Z., Wang, S., Chi, Y., and Yan, J., 2015. "Catalytic pyrolysis of petroleum sludge for production of hydrogen-enriched syngas." *Int. J. Hydrogen Energy 40*, 16077–16085.

Ibrahim, S.A., Ekinci, E.K., Karaman, B.P., and Oktar, N., 2021. "Coke-resistance enhancement of mesoporous γ-Al_2O_3 and MgO-supported Ni-based catalysts for sustainable hydrogen generation via steam reforming of acetic acid." *Int. J. Hydrogen Energy 46*, 38281–38298.

Jia, H., Zhao, S., Zhou, X., Qu, C., Fan, D., and Wang, C., 2017. "Low-temperature pyrolysis of OS: Roles of Fe/Al-pillared bentonites." *Arch. Environ. Prot. 43*, 82–90.

Jin, X., Teng, D., Fang, J., Liu, Y., Jiang, Z., Song, Y., Zhang, T., Siyal, A.A., Dai, J., Fu, J., Ao, W., Zhou, C., Wang, L., and Li, X., 2021. "Petroleum oil and products recovery from OS: Characterization and analysis of pyrolysis products." *Environ. Res. 202*, 111675.

Kasmin, N.H., Zubairi, S.I., Lazim, A.M., and Awang, R., 2020. "Thermal treatments on the oil palm fruits: Response surface optimization and microstructure study." *Sains Malaysiana 49*, 2301–2309.

Lee, Y., Shin, J., Kwak, J., Kim, S., Son, C., Cho, K., Chon, K. 2021. "Effects of NaOH activation on adsorptive removal of herbicides by biochar prepared from ground coffe residues: A review." *Int. J. Energy Res.* 14, 1297.

Li, J., Lin, F., Li, K., Zheng, F., Yan, B., Che, L., Tian, W., Chen, G., and Yoshikawa, K., 2021. "A critical review on energy recovery and non-hazardous disposal of OS from petroleum industry by pyrolysis." *J. Hazard. Mater. 406*, 124706.

Lin, B., Wang, J., Huang, Q., Ali, M., and Chi, Y., 2017a. "Aromatic recovery from distillate oil of OS through catalytic pyrolysis over Zn modified HZSM-5 zeolites." *J. Anal. Appl. Pyrolysis 128*, 291–303.

Lin, B., Wang, J., Huang, Q., and Chi, Y., 2017b. "Effects of potassium hydroxide on the catalytic pyrolysis of OS for high-quality oil product." *Fuel 200*, 124–133.

Liu, C., Hu, X., Xu, Q., Zhang, S., Zhang, P., Guo, H., You, Y., and Liu, Z., 2021. "Response surface methodology for the optimization of the ultrasonic-assisted rhamnolipid treatment of OS." *Arab. J. Chem. 14*.

Lu, F., Chen, X., Lei, Z., Wen, L., and Zhang, Y., 2021. "Revealing the activity of different iron carbides for Fischer-Tropsch synthesis." *Appl. Catal. B Environ. 281*, 119521.

Murungi, P.I., and Sulaimon, A.A., 2022. "Petroleum sludge treatment and disposal techniques: a review." *Environ. Sci. Pollut. Res. 29*, 40358–40372.

Naidu, B.N., Kumar, K.D.P.L., Saini, H., Kumar, M., Kumar, T.N., and Prasad, V.V.D.N., 2022. "Coke deposition over Ni-based catalysts for dry reforming of methane: effects of MgO-Al_2O_3 support and ceria, lanthana promoters." *J. Environ. Chem. Eng. 10*, 106980.

Nazarudin, Jayanti, N., Alfernando, O., Prabasari, I.G., Ulyarti, and Sarip, R., 2020. "Catalytic cracking of polyethylene terephthalate (PET) plastic waste and palm fibre mixtures using Ni-USY zeolite catalyst." *J. Phys. Conf. Ser. 1567*.

Okoronkwo, E.A., Imoisili, P.E., Olubayode, S.A., and Olusunle, S.O.O., 2016. "Development of Silica Nanoparticle from Corn Cob Ash." *Adv. Nanoparticles 05*, 135–139.

Oyebanji, J.A., Okekunie, P.O., Itabiyi, O.E., 2023. " Box Behnken design application for optimization of bio-oil yield from catalytic pyrolysis of agro-residue." *Fuel Communications. 16*, 100091.

Saravanan, S and Dubey, R.S. 2020. Romanian Journal. 105 - 112.

Sharma, S.K., Verma, D.S., Khan, L.U., Kumar, S., and Khan, S.B., 2018. "Handbook of Materials Characterization." *Handb. Mater. Charact.* 1–613.

Shi, S., 2018. "Advances in modeling hydrocarbon cracking kinetic predictions by quantum chemical theory: A review." *Int. J. Energy Res. 42*, 3164–3181.

Tran, T.N., Pham, T.V., Le, M.L., Nguyen, T.P., Tran, V.M. 2013. " Synthesis of amorphous silica and sulfonic acid functionalized silica used as reinforced phase for polymer electrolyte membrane." *Adv. Nat. Sci.: Nanosci. Nanotechnol. 4,* 045007

Triyono, T., Trisunaryanti, W., Falah, I., Rahmi, L. 2023. "Effect of acetic acid and/or sodium hydroxide treatment towards characters of wonosari natural zeolite for hydrotreatment of castor oil into biofuel." *Indones. J. Chem. 23*, 298 -308.

Tsiotsias, A.I., Charisiou, N.D., Sebastian, V., Gaber, S., Hinder, S.J., Baker, M.A., Polychronopoulou, K., and Goula, M.A., 2022. "A comparative study of Ni catalysts supported on Al_2O_3, MgO–CaO–Al_2O_3 and La_2O_3–Al_2O_3 for the dry reforming of ethane." *Int. J. Hydrogen Energy 47*, 5337–5353.

Wang, J., Lin, B.C., Huang, Q.X., Ma, Z.Y., Chi, Y., and Yan, J.H., 2017. "Aromatic hydrocarbon production and catalyst regeneration in pyrolysis of OS using ZSM-5 zeolites as catalysts." *Energy and Fuels 31*, 11681–11689.

Zhang, X., Xu, J., Ran, S., Gao, Y., Lyu, Y., Pan, Y., Cao, F., Lin, Y., Yang, Z., Wang, Z., Guo, D., Wang, Q., Zhu, L., and Zhu, Y., 2022. "Experimental study on catalytic pyrolysis of OS for H_2 production under new nickel-ore-based catalysts." *Energy 249*, 123675.